Volume Dependence of Molecular Flexibility in Poly(ethylene oxide) under Negative Pressure

S. Neyertz,* D. Brown, D. Colombini, N. D. Albérola, and G. Merle

Laboratoire des Matériaux Polymères et Composites, LMPC (UMR-CNRS 5041), Université de Savoie, Savoie Technolac, 73376 Le Bourget-du-Lac Cedex, France

Received June 10, 1999; Revised Manuscript Received October 5, 1999

ABSTRACT: We use here molecular dynamics (MD) simulations to study the structure and mobility of bulk melt PEO at the molecular level in response to a volume expansion such as might occur at the interphase of compatibilized polymer blends. PEO is simulated under constant-pressure conditions and compared to lower density constant-volume systems in the range ∼90−100% of the ambient pressure density at 343 K. Analyses include energies and pressure, conformational data, intra- and intermolecular structural features, and the evolution of chain mobility and mechanical properties. The decrease in density induces negative pressures and an increase in molecular mobility. Moreover, a decrease of 10% in density is found to correspond to a temperature shift of approximately 60 K for the polymer backbone torsional interconversion relaxation times around C−O bonds.

1. Introduction

The pressure (*P*), volume (*V*), and temperature (*T*) are three fundamental parameters in polymers. Although attention is usually focused on *T*, *P* or, alternatively, *V* can also affect polymer properties. Indeed, volume effects can appear in polymer blends and act in terms of molecular mobility.

Most polymers are thermodynamically immiscible and form heterogeneous multiphase systems with weak physical and chemical interactions between the phases and poor properties. An improvement is achieved by introducing a so-called compatibilizer, such as a block or graft copolymer, which interacts with the other polymers and so offers new properties to the blends.[1−3] This process often results in a stable and finer dispersion of the minor component into the other and leads to the formation of an interphase zone between the continuous and dispersed phases.[4]

It was recently found that the addition of a poly(styrene-*graft*-ethylene oxide) (P(S-*g*-EO)) compatibilizer in poly(2,6-dimethyl-*p*-phenylene oxide) and poly(methyl methacrylate) (PPO/PMMA) blends results in a new loss peak in the mechanical spectra of the blends.[5−8] The tan δ peak appears in a distinctive temperature region of the ternary blend and cannot be explained by a molecular transition in any of the pure components.[5] This phenomenon was thus attributed to the existence of an interphase with its own characteristic properties and was referred to as a "micromechanical transition" in order to distinguish it from other molecular transitions.[6] This new "transition" was also predicted by an interlayer mechanical model, which simulated the viscoelastic response of immiscible polymer blends separated by an interphase, using just the properties of its pure components.[5] The interphase Poisson's ratio was found to influence strongly the position of the "micromechanical transition" in the theoretical dynamic mechanical spectra (DMS), thus indicating that the compressibility of the interphase could have a key role in the viscoelastic response of thermoplastic blends. In a similar vein, Colombini et al.[9] detailed the observation of a "micromechanical transition" in a compatibilized thermoset/thermoplastic blend and showed that it was strongly dependent on the thermal history of the sample. They studied the influence of several thermal treatments on the amplitude and temperature behavior of the additional loss peak and suggested that viscoelastic behavior could be directly associated with the expansion of the components.[9]

In this paper, we present a different approach to the problem in employing molecular dynamics (MD) simulations.[10] These provide information at the atomistic level by integrating Newton's equations of motion for all the atoms in a model of the system. While in principle it is possible to create an explicit model of the ternary thermoplastic PPO/PMMA/P(S-*g*-EO) blend, extremely complex many-body potentials would be needed to properly represent the interactions through the full interphase. It is thus more feasible to study the different components on their own and then progressively combine their potential parameters to eventually make up the full system.

We have previously developed a fully atomistic optimized model for poly(ethylene oxide), PEO, by accurately reproducing its behavior in the crystalline and in the bulk melt phases.[11−13] Since PEO is part of the P(S-*g*-EO) interphase in the (PPO/PMMA) thermoplastic blends,[5−8] we study here, as a first step, the dependence of its properties in response to a volume expansion such as might occur at the interphase of the blend. We make no attempt here to justify how such a volume expansion might come about. The calculations presented here on PEO consider it to be in its bulk state, and other factors, such as edge effects or the confinement state of the molecules,[14,15] are not taken into account. Indeed this work is aimed primarily toward the analysis of the effect of isotropic negative pressure, which is known experimentally to decrease the glass transition temperature.[16] Despite the ease with which negative pressures can be created in molecular dynamics simulations employing

* To whom correspondence should be addressed. E-mail Sylvie.Neyertz@univ-savoie.fr.

10.1021/ma990927n CCC: $19.00
Published on Web 02/22/2000

periodic boundary conditions, they have, to date, rarely been used deliberately to study systems in these conditions. While work on silica glass,[17] water,[18] and cavitation in an *n*-octane fluid[19] have been reported, the present paper is, to our knowledge, the first to deal with the molecular structure and mobility of an amorphous polymer under isotropic negative pressure.

The glass transition temperatures of PPO, PMMA, and P(S-*g*-EO) suggest that the interphase component is in the rubbery state while PPO and PMMA remain in the vitreous state at 70° C (343 K) and 4×10^{-3} Hz, which corresponds to the temperature of the "micromechanical transition".[5] Since the thermal expansion coefficient of a rubber phase is roughly 10 times larger than that of a polymeric glass, we estimated the volume variation of the blend interphase upon cooling from 260° C to room temperature at a maximum of ∼10%. PEO was thus simulated in the range ∼90−100% of its ambient pressure density at 343 K, which is close to the temperatures of the experimentally determined "micromechanical transition",[6,9] in order to assess the effect of volume expansion on its structure and dynamics.

The details of the simulations are given in section 2. The effects of volume expansion on the polymer chains are analyzed in section 3.

2. Details of the Simulations

2.1. The PEO Model. Extensive details of our PEO model have been given previously.[11−13,20] The potential energy of the system was described in terms of angle-bending deformations, torsional motions around the backbone dihedral angles, and van der Waals and electrostatic interactions. $H-(CH_2-CH_2-O)_{30}-C_2H_5$ was chosen as the basic chemical PEO formula, since Eklind et al. reported an average number of monomers, n_m, of 30 for the PEO side chains in their P(S-*g*-EO) graft polymer.[6]

We used a growth procedure based on pivot Monte Carlo (PMC) sampling of the bond angle and torsional configurational phase space, which has also been discussed elsewhere.[13,20−23] Ten uncorrelated structures of a 92 backbone-atom chain ($n_m = 30$) were generated by the PMC procedure in order to obtain a system of several molecules, which contained 2180 atoms in total. The chains were then randomly reorientated and distributed in a periodic cubic MD box with side length L chosen to give an initial density of 1100 kg m^{-3}, which was close to the experimentally estimated value for bulk PEO.[24,25]

All MD simulations were performed using the *gmq* MD program,[26] either in its scalar form on SGI O2 workstations or in its parallel domain decomposition form (*ddgmq*)[27] on the Cray T3E of the IDRIS center (Orsay, France) and IBM SP2 of the CNUSC center (Montpellier, France). The time step used was 1 fs. The initial system was first equilibrated under constant-volume NVT conditions. It was then switched to NpT conditions, in which the isotropic pressure was maintained at the required value of 1 bar by loose coupling with a τ_P of 5 ps,[28] and the box was kept cubic. The truncation radius for Buckingham and for the real-space part of the electrostatic potential interactions, R_{cutoff}, was set throughout at $L/2$ and thus varied with time. Long-range corrections to the energy and the pressure were made on the assumption that $g(r) = 1$ beyond the cutoff.[10] Optimum convergence of the total Ewald sum[29] in reasonable time was obtained by using a separation parameter, $\alpha = 0.30$ Å^{-1}, and a reciprocal space cutoff, $K_{max} = 8$.[13] The average temperature was kept close to 343 K by weak coupling to a heat bath,[30] with a τ_T of 0.1 ps. The equilibration run was carried out until the density stabilized. Mechanical and conformational equilibrium was reached on a time scale of ∼100 ps.

2.2. Production Runs. The equilibrated simulation at $T \sim 343$ K and $p \sim 1$ bar was extended up to 1000 ps. Four other samples with densities equal to 990, 1017.5, 1050, and 1072.5 kg m^{-3} were created by increasing the size of the cubic simulation box and allowing the systems to relax under constant-volume conditions while keeping $T \sim 343$ K. Each of the lower density runs was extended to a production time of 500 ps.

To assess whether the number of molecules influenced the results, a larger 17 440-atom cubic MD cell containing 80 PEO molecules was also created by replicating eight times the system equilibrated under ambient pressure conditions. It was simulated under constant-volume conditions for 200 ps using the domain decomposition parallel version of the *gmq* program, *ddgmq*.[26,27] The truncation radius for Buckingham interactions and the real-space part of the electrostatic potential were reset to ∼8.1 Å, and the reciprocal space cutoff, K_{max}, was increased to 14 to reach convergence.

In all cases, configurations were stored for postanalysis at 5 ps intervals and thermodynamic and conformational data every 0.5 ps. Analyses were conducted on the last 500 ps of each run, except for the 17 440-atom run which was studied over its last 150 ps. A schematic representation of the relaxed 2180-atom PEO bulk melt sample under ambient pressure conditions is shown in Figure 1.

In a second series, five shorter MD simulations were carried out under N**P**T constant-pressure *tensor* conditions by first setting the externally applied on-diagonal pressure tensor components to the equilibrium average pressure for each system under study and the off-diagonal components to zero. The rate of change of the externally applied pressure tensor component along the z direction, P_{zz}, was then changed to −2.5 MPa ps^{-1}. The internally measured pressure tensor, **P**, was loose-coupled to the externally applied pressure tensor with a coupling constant of 5 ps,[28] and both the size and the shape of the boxes were allowed to vary over periods of 150 ps each. The elongations of MD boxes were subsequently recorded in order to calculate Young's moduli as a function of the density.

3. Results and Discussion

Isotropic negative pressures are not routinely accessed experimentally, and so, in comparison to compression, relatively little is known about the states of matter under isotropic tension. Angell et al. adapted techniques dating from the work of Berthollet in the 1850s[31] to vitrify the glass-forming liquid *o*-terphenyl under negative pressure in order to preserve the stretched configurational state.[16] These authors compared the temperature range over which stretched, ambient pressure, and compressed glasses return to equilibrium and showed that there was a much broader spread of relaxation times for the former. More precisely, the beginning of the structural recovery process of the stretched glass is at much lower temperatures (equivalent to high frequencies), which reveals a sharp increase in molecular mobility. Significantly, they found

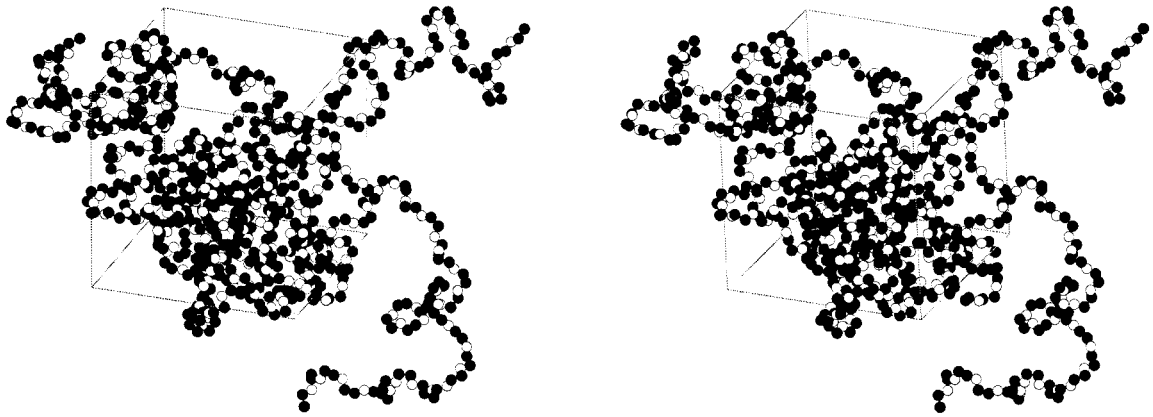

Figure 1. Stereoview of the PEO melt sample at its normal density at $T = 343$ K. Open and filled spheres are respectively oxygens and carbons. Hydrogens are omitted for clarity.

Table 1. Details of the Simulations Undertaken at 343 K for PEO at Different Densities[a]

no. of atoms	2180	2180	2180	2180	2180	17440
$\langle\rho\rangle$	990	1017.5	1050	1072.5	1110 ± 1	1109
specific volume	1.0101	0.9828	0.9524	0.9324	0.9009 ± 0.0008	0.9017
$\langle U\rangle$	−19.20	−19.92	−20.59	−20.96	−21.76	−21.786
$\langle U_{pot}\rangle$	−28.07	−28.79	−29.46	−29.83	−30.63	−30.673
$\langle U_{bend}\rangle$	4.35	4.35	4.35	4.35	4.35	4.351
$\langle U_{tors}\rangle$	5.98	5.94	5.94	6.15	6.19	6.213
$\langle U_{Buck}\rangle$	−20.08	−20.71	−21.42	−21.88	−22.64	−22.531
$\langle U_{coul}\rangle$	−18.33	−18.37	−18.33	−18.45	−18.54	−18.707
$\langle U_{pot}^{inter}\rangle$	−18.79	−19.25	−20.63	−20.84	−21.59	−21.552
$\langle U_{Buck}^{inter}\rangle$	−16.57	−17.03	−18.12	−18.41	−19.08	−19.037
$\langle U_{coul}^{inter}\rangle$	−2.22	−2.22	−2.51	−2.43	−2.51	−2.515
$\langle p\rangle$	-212 ± 7	-197 ± 4	-155 ± 3	-104 ± 4	0 ± 1	9 ± 2
⟨% trans⟩ OCCO	10.7	10.7	12.0	12.2	12.7	11.7
⟨% trans⟩ CCOC	83.2	83.2	83.4	81.8	81.1	81.4

[a] The average (or fixed) density $\langle\rho\rangle$, pressure $\langle p\rangle$, and specific volume of each run are given respectively in kg m^{-3}, MPa, and cm^3 g^{-1}. The average total $\langle U\rangle$ and potential $\langle U_{pot}\rangle$ energies, as well as the different contributions to the potential energy, are quoted in kJ/mol of monomer with a maximum error of 0.05 for the 2180-atom systems and 0.005 for the 17 440-atom system. The "total" label refers to both intramolecular and intermolecular energies, while the "inter" label refers only to intermolecular contributions. Also shown are the mean percentage of trans conformers for backbone OCCO and CCOC torsion angles with a maximum error of 0.04.

an average relaxation time at least 10^3 shorter than what would be expected on the basis of extrapolating data for the effect of compression on relaxation times. Angell et al. attributed this phenomenon to a marked asymmetry in the response of the structural relaxation times to negative and positive pressures.[16]

It could also be interesting to consider the *volume* dependence of relaxation times in this region. The compressibility increases very rapidly at negative pressures until in fact a divergence is reached at the tensile limit; experimentally, it is difficult to attain this limit with macroscopic samples as cavitation usually occurs. The important point is that below zero pressure volume increases much faster for an equal change in pressure than above zero pressure, and it is very likely that this effect plays an important role in the large change in relaxation times.

In computer simulations, the use of periodic boundary conditions makes accessing regions of negative pressure very much less of a problem. We thus attempt to characterize hereby the key features of our PEO model held under negative pressures.

3.1. Thermodynamic Data. The density of each system under study is given in Table 1 along with the corresponding energies and pressures. The results for the 17 440-atom system are comparable to those for the corresponding 2180-atom system equilibrated under ambient pressure conditions, thus suggesting that the number dependence is very minor. The pressure difference between both is relatively small in MD terms, but several factors could contribute to this difference. First, the larger system was built from a particular 2180-atom configuration which happened to have a density of 1109 kg m^{-3} and subsequently run under NVT conditions, rather than NpT, for a shorter time. Second, in changing system size, the Ewald summation parameters were also reoptimized. This slightly altered the real space cutoff so some small direct (force evaluation) and indirect consequences (cutoff corrections) are expected.

The only fluctuation in density occurs in the system equilibrated under ambient pressure conditions since its MD cell was allowed to change size at 343 K in response to the desired applied pressure of 1 bar. Once equilibrated, these fluctuations were centered around the well-defined mean of 1110 kg m^{-3}. This value is in very close agreement with the density of liquid PEO estimated according to an empirical expression for the molar volume of V_l as a function of temperature T given by Van Krevelen:[25]

$$V_l(T) \approx V_w(1.30 + 10^{-3}T) \qquad (1)$$

$V_w = 24.16$ cm^3 mol^{-1} for PEO, V_l (343 K) = 39.69 cm^3 mol^{-1}, and the estimated density at 343 K is 1111 kg m^{-3}. Experimental findings for linear poly(ethylene oxide) of molecular weight ∼400 (8 or 9 monomers) give densities of the order of 1130 kg m^{-3} at 273 K.[32] With experimental values for the molar thermal expansivity

of liquid PEO in the range (273−291) × 10^{-4} cm^3 mol^{-1} K^{-1},[25] the corresponding densities at 343 K are of the order of 1090 kg m^{-3}. The MD model used in this study thus reproduces well the actual density of molten PEO at 343 K.

In previous studies using the same model of PEO at 400 K, the linear relation between the density and the inverse number of backbone atoms in the chains was established.[13,23] For the current chain length of n_m = 30, the previous results (see Figure 2 of ref 13) predict a density of ∼1065 kg m^{-3} at 400 K. Extrapolating linearly from this predicted result at 400 K and the value of 1110 kg m^{-3} found here, the temperature that would give the lowest density studied of 990 kg m^{-3} would be 494 K, i.e. ∼150 K higher. Using the Van Krevelen equation, an even higher estimate of 544 K is obtained, i.e. ∼200 K higher. This puts into perspective the fact that the range of volume expansions studied is quite large. Even so, the point here is to establish the quantitative variation of properties under volume expansion, and we thus chose to cover a wider rather than narrower range.

As seen in Table 1, the average energies increase linearly upon volume expansion. The "total" energy results relate to both intra- and intermolecular interactions, while the "inter" results are the intermolecular energies. $\langle U \rangle$ represents the total energy, i.e. the sum of kinetic and potential energies. As expected for systems at the same temperature, the constant difference between $\langle U \rangle$ and the total average potential energy $\langle U_{pot} \rangle$ confirms that the kinetic contribution is the same for all simulations. The variations in $\langle U \rangle$ are actually directly proportional to the variations in the intermolecular van der Waals interactions, $\langle U^{inter}_{Buck} \rangle$. Near-neighbor intramolecular bending interactions, $\langle U_{bend} \rangle$, are not affected by the change in volume, as these stiff harmonic degrees of freedom are mainly related to the temperature. The intramolecular torsional $\langle U_{tors} \rangle$ energy diminishes slightly in the lower density systems, which suggests small conformational changes (see below). The electrostatic $\langle U_{coul} \rangle$ energy is mostly due to intramolecular interactions and varies very little, with a conservation of the balance between repulsive like-charges and attractive unlike-charges interactions. As the van der Waals radii of the atoms are kept constant, the total energy change can thus be largely attributed to the increase in volume and the reduction of the net attractive ($1/r^6$) interaction. It is interesting to note that the density dependence of the total energy is governed by excluded volume even in a polymer such as PEO, where Coulombic interactions are an important part of the total potential energy.

The P−V curve for the PEO melts at 343 K, i.e. the specific volume as a function of the average pressure $\langle p \rangle$, is displayed in Figure 2. The open squares in Figure 2 correspond to the MD volume expansion results given in Table 1. The filled squares are experimentally determined data for long-chain molten PEO (M_w = 200 000 g/mol).[33] The experimental data are in good agreement with the Simha−Somcynsky[34] and Tait[35] equations of state (EOS).[33] The curve for the latter, obtained with the Tait EOS parameters of Schmidt and Maurer,[33] is also shown for comparison in Figure 2 and has been extrapolated below zero despite the questionable validity of the EOS for negative pressures. The average pressure in the MD models is almost a continuation of the experimental positive pressure data, with

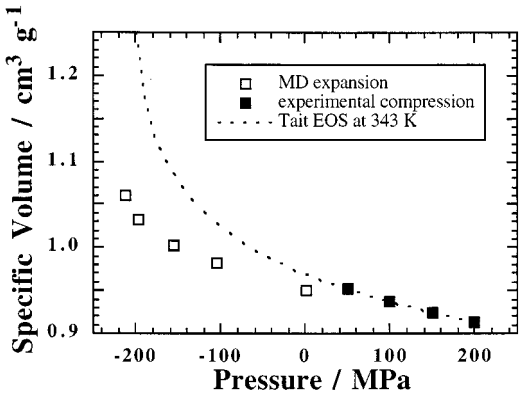

Figure 2. Specific volume in cm^3 g^{-1} of PEO as a function of the average pressure in MPa at a temperature of T = 343 K. The open squares correspond to the volume expansion results obtained in our model. The filled squares are experimentally measured compression data which have been derived from the results published in ref 33. Also shown for comparison is the Tait[35] EOS at 343 K obtained using the parameters of Schmidt et al.[33]

the slight offset probably arising from differences in the lengths of the chains. Qualitatively, it follows the general behavior "predicted" by the Tait EOS for negative pressures. The simulated pressure decreases with increasing specific volume and tends toward a limiting value, the tensile limit, at which the compressibility diverges toward infinity. This corresponds to a value of at least −220 MPa. This order of magnitude is directly comparable to the internal pressure which is in the range 240−260 MPa for various polymers.[25] For systems with a lower density, it is inevitable that $\langle p \rangle$ will rise again in order to reach zero at the infinite expansion limit. Within this context, it should be noted that the Tait equation reaches an asymptotic limiting value[35] as the volume increases, rather than passing through a minimum and, as such, cannot be a valid representation for PVT data at volumes beyond the tensile limit. The specific volume change of ∼0.056 cm^3 g^{-1} induced by a compression from 0 to 200 MPa[33] is much smaller compared to that of ∼0.110 cm^3 g^{-1} in our expansion from 0 to −200 MPa. Negative and positive pressure changes of this magnitude do not act symmetrically on the specific volume of the melt, a consequence of the divergent compressibility at negative pressures.

3.2. Molecular Structure and Conformational Properties. 3.2.1. Backbone Dihedral Angle Distributions. Table 1 gives the ⟨% trans⟩ for both C−C and C−O backbone dihedral angles as a function of the density. Please note that we use the dihedral angle convention where τ is gauche$^-$ (g^-) if $-180° \le \tau \le -60°$, trans (t) if $-60° < \tau < 60°$, and gauche$^+$ (g^+) if $60° \le \tau \le 180°$. As expected, the OCCO ⟨% trans⟩ reflects the well-known gauche effect in PEO, i.e. the fact that torsions around C−C bonds are mainly found in the gauche state, while the CCOC angles tend to favor the trans state.[36,37] It is clear from Table 1 that this static property is not very much affected by the change in pressure. The C−C ⟨% trans⟩ decreases slightly with the density, which corresponds to an increase in gauche states and coiled conformations at lower density. On the other hand, the C−O ⟨% trans⟩ is seen to increase, which would have the inverse effect. Despite these minor overall changes in the equilibrium conformations, both angles have the same tendency, i.e. increasing their population in their lower energy wells as density decreases.

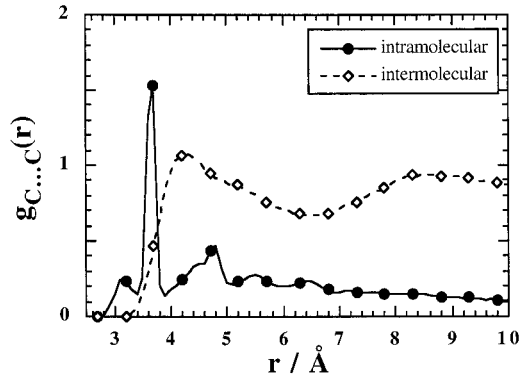

Figure 3. Intramolecular and intermolecular contributions of the C···C radial distribution functions for the PEO bulk melt sample at its normal density.

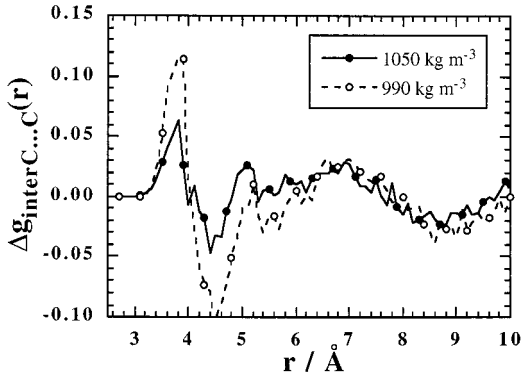

Figure 4. Function $\Delta g_{inter}(r)$ plotted for C···C interactions for two lower density systems. This function gives the difference between the actual rdf at the lower densities and that expected on the basis of an affine scaling of the normal density results (see text for details). The scaling of the structure is noticeably less affine in the nearest-neighbor shells.

3.2.2. Radial Distribution Functions. Radial distribution functions were determined to characterize the local environment within a radius of about 10 Å. These so-called $g(r)$ functions are a spherically averaged one-dimensional representation of a three-dimensional structure and are traditionally used in the structure determination of amorphous materials. Both intramolecular $g_{intra}(r)$ and intermolecular $g_{inter}(r)$ contributions to the total radial distributions functions can be computed to facilitate identification of the peaks.

The intra- and intermolecular radial distribution functions for backbone C···C interactions in the bulk melt sample at the normal density at 343 K are displayed in Figure 3. The large narrow peaks due to C−C bonds at 1.54 Å and COC bends at 2.3 Å have been omitted for clarity in the C···C $g_{intra}(r)$. The first peaks visible in Figure 3 are related to the COCC torsional potential, with the gauche state at ∼3.0 Å being less populated than the trans state at ∼3.7 Å. OCCO torsions can be similarly analyzed in the O···O $g_{intra}(r)$ with a much larger peak for their gauche state than for their trans state. The next peak at ∼3.7 Å in the C···C $g_{intra}(r)$ is due to "1···5" C···C interactions brought about by the neighboring "1···5" attractive C···O interactions along the chains.[20] The nearest-neighbor intermolecular structure occurs for C···C interactions at about 4 Å, and the correlation decays at larger distances.

To compare the influence of density on the local environment of the chains, both $g_{intra}(r)$ and $g_{inter}(r)$ functions were calculated for all other systems under study. Results for the ambient pressure density system were also used to obtain "theoretical" results at lower densities, to normalize for the simple volume scaling contributions to the $g(r)$. To obtain theoretical $g_{intra}(r)$, we made the assumption that the intramolecular interatomic distances were unaffected by volume scaling, as should for example be the case for rigid bonds. This gave $g_{intra}^{theor}(V_2,r) = g_{intra}(V_1,r)V_2/V_1$, where V_1 and V_2 are the volumes of the MD box at the reference and lower densities, respectively. For the $g_{inter}(r)$, we assumed an affine scaling of the structure, i.e. that intermolecular interatomic distances were scaled with volume change. This translates to a prediction of the form $g_{inter}^{theor}(V_2,r) = g_{inter}(V_1,r(V_1/V_2)^{1/3})$. The theoretical radial distribution functions generated from the normal density results in the above ways were then subtracted from the actual $g(r)$ found at the lower densities, and the resulting $\Delta g(r)$ functions were analyzed. $\Delta g_{intra}(r)$ for C···C and O···O interactions (results not shown) exhibit the change predicted by conformational averages, i.e. an increase in height for peaks corresponding to gauche OCCO and trans COCC angles as the system expands. Variations in the intermolecular structure can also be seen in the $\Delta g_{inter}(r)$ functions, examples of which are given in Figure 4 for the C···C interactions. The trend is the same for all systems under study. The affine scaling assumption works well at large separations, but at the nearest-neighbor distances, there is clearly a discernible tendency for the atoms to "fall back" into the potential wells, i.e. a nonaffine or more intramolecular type behavior.

3.2.3. Void Distribution. To see whether cavitation occurred in our model systems, the distribution and amount of "void space" were examined. To do this, probes, with a radius of 2 Å, were randomly inserted into each of the configurations stored every 5 ps during the MD simulations. Those probes that did not overlap with any of the atoms of the polymer chains were counted, and their positions were plotted three-dimensionally in order to visualize the voids. A total of 200 000 trial insertions per configuration was found to give reliable results. A visual examination of the void distribution did not reveal any tendency for cavitation. With the 2 Å probe, the percentage of accepted insertions (= percentage of void space) was 5.30% for 990 kg m^{-3}, 4.00% for 1017.5 kg m^{-3}, 2.87% for 1050 kg m^{-3}, 2.22% for 1072.5 kg m^{-3}, and 1.15% for 1110 kg m^{-3}, i.e. an almost linear increase in the void space with the volume.

3.3. Molecular Mobility. 3.3.1. Conformational Correlations. To evaluate the effect of the density on chain mobility, relaxation functions of the form

$$R_{TT}(t) = \langle H_T\{\tau_i(0)\}H_T\{\tau_i(t)\}\rangle \qquad (2)$$

and

$$R_{G\pm G\pm}(t) = \frac{\langle H_G^-\{\tau_i(0)\}H_G^-\{\tau_i(t)\}\rangle + \langle H_G^+\{\tau_i(0)\}H_G^+\{\tau_i(t)\}\rangle}{2} \qquad (3)$$

where $\tau_i(t)$ is the value of dihedral angle i at time t and $H_T\{\tau_i(t)\}$, $H_G^-\{\tau_i(t)\}$, and $H_G^+\{\tau_i(t)\}$ are the characteristic functions of the trans, gauche$^-$, and gauche$^+$ states, respectively, were computed. $H_T\{\tau_i(t)\}$, $H_G^-\{\tau_i(t)\}$, and

Table 2. Best Fit Parameters for the $C_{TT}(t)$ Relaxation Functions for CCOC Torsions to the Stretched Exponential (KWW) Form, $\exp(-(t/\tau)^{\beta})$

ρ/kg m^{-3}	1110	1072.5	1050	1017.5	990
τ/ps	33.7(1)[a]	21.5(2)	14.8(1)	10.1(1)	8.41(3)
β	0.331(1)	0.250(1)	0.300(1)	0.323(1)	0.355(1)

[a] The numbers in parentheses are the errors in the last figure as reported by the nonlinear least-squares regression routine.

$H_G^+\{\tau_i(t)\}$ each take only two values:

$$H_T\{\tau_i(t)\} = 1 \qquad \text{if } -60° < \tau_i(t) < 60° \qquad (4a)$$

$$H_G^-\{\tau_i(t)\} = 1 \qquad \text{if } -180° \le \tau_i(t) \le -60° \qquad (4b)$$

$$H_G^+\{\tau_i(t)\} = 1 \qquad \text{if } 60° \le \tau_i(t) \le 180° \qquad (4c)$$

and zero otherwise. The method has been presented in detail elsewhere[38] and provides a reliable method for assessing the degree of conformational equilibrium in a system. Most useful are the normalized forms of the correlation functions, $C_{TT}(t)$ and $C_{G\pm G\pm}(t)$, which are defined as

$$C_{TT}(t) = \frac{R_{TT}(t) - \langle X_T\rangle^2}{\langle X_T\rangle - \langle X_T\rangle^2} \qquad (5)$$

$$C_{G\pm G\pm}(t) = \frac{R_{G\pm G\pm}(t) - \langle X_{G\pm}\rangle^2}{\langle X_{G\pm}\rangle - \langle X_{G\pm}\rangle^2} \qquad (6)$$

where $\langle X_T\rangle = R_{TT}(0)$ is the mean trans fraction and $\langle X_{G\pm}\rangle = R_{G\pm G\pm}(0)$ is the mean gauche fraction. To achieve better statistics, the normalized correlation functions for OCCO and CCOC backbone torsions were calculated for their most common conformational states, i.e. $C_{G\pm G\pm}(t)$ and $C_{TT}(t)$, respectively. They are displayed in Figure 5a,b for the systems under study. All plots show the same general trend toward higher polymer chain flexibility as the density decreases. The intrinsic conformational states of the chains become uncorrelated faster at lower densities. The kinetics of OCCO relaxation rates are slower than their CCOC counterparts, which has been attributed[13] to the steeper well barriers for OCCO transitions (10.04 kJ mol^{-1}) with respect to CCOC transitions (7.53 kJ mol^{-1}).[39] Local motion is thus more likely to originate from CCOC than from OCCO units.

To obtain quantitative estimates of the relaxation times, we attempted to fit the relaxation functions to the stretched exponential (KWW) form $\exp(-(t/\tau)^{\beta})$.[40] The fits of the $C_{TT}(t)$ data for CCOC torsions were remarkably good, and the best fit parameters are shown in Table 2 for each of the densities under study. The τ decrease systematically with density while the β factors vary in the range from 0.25 to 0.35, but with no discernible trend. Similar fits were attempted for the OCCO $C_{G\pm G\pm}(t)$, but these were less good. The fact that there are half as many of these torsions and that they relax much slower than the CCOC torsions probably contributes to this. In what follows, we focus on the CCOC torsions which, in any case, relax significantly faster, are twice as numerous, and thus contribute much more to the overall relaxation of the chains.

The data for the fitted τ presented in Table 2 are plotted in Figure 6 as a function of the specific volume. The smooth line shown is a fit of the data to the WLF

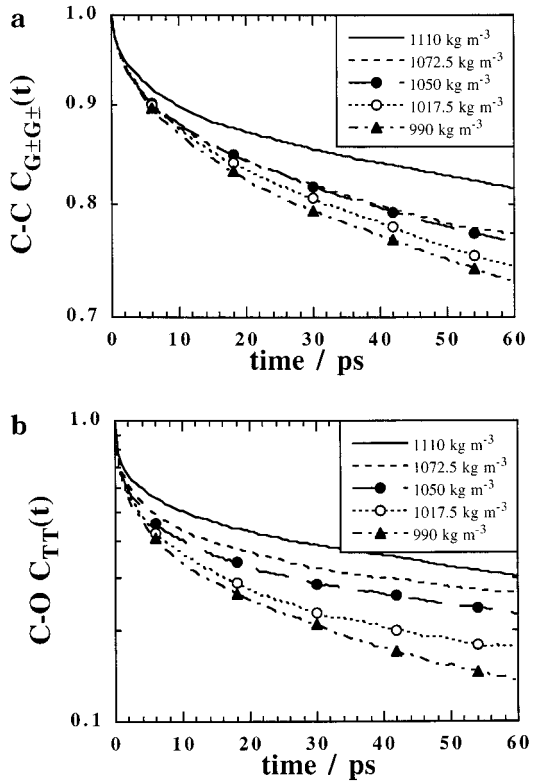

Figure 5. Normalized forms of the relaxation functions $C_{G\pm G\pm}(t)$ and $C_{TT}(t)$, for OCCO (a) and CCOC (b) backbone angles, respectively, as a function of density.

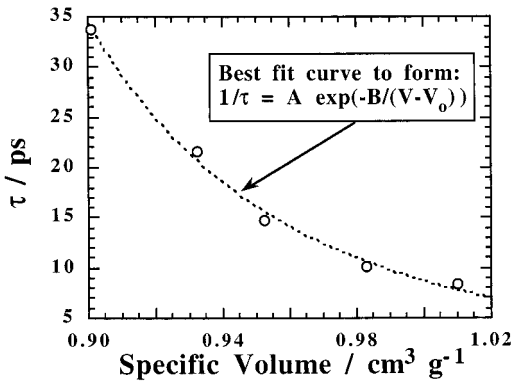

Figure 6. Relaxation times obtained from least-squares fits to the stretched exponential form of the CCOC $C_{TT}(t)$ data (b) plotted as a function of specific volume. The smooth dotted line shown is a fit of the data to the empirical form $1/\tau = A \exp(-B/V - V_0)$ with $A = 51.869$, $B = 3.333$, and $V_0 = 0.454\,81$.

form $1/\tau = A \exp\{-B/(V - V_0)\}$. To interpret the change in relaxation time with volume, we then converted it into an equivalent change in temperature in the following manner. Previously published data for the same PEO basic model at ambient pressures exists for both longer chains, with $n_m = 143$ EO monomers, at 400 and 500 K[41] and for a range of shorter PEO homologues, from $n_m = 2$ to 10 EO units, at 400 K.[13,23] The polymer followed a classical behavior; i.e., chain mobility increased with temperature. The $C_{TT}(t)$ data for CCOC torsions for all these chains also fit well to the stretched exponential form. From the data for all chain lengths at 400 K, it was first established whether it was reasonable to assume that the relaxation time for the $n_m = 30$ chains were close to the near-asymptotic value of the long chain. Indeed, it was found that this was the case as, to a very good approximation, the best-fit τ

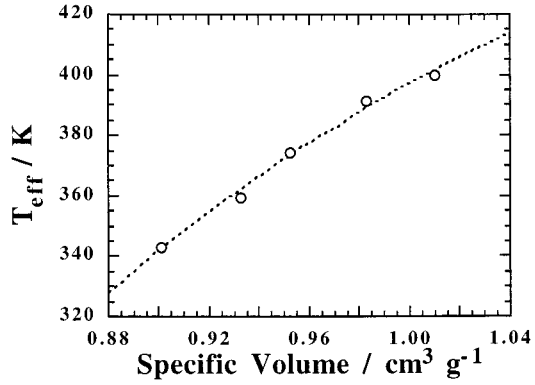

Figure 7. Effective temperature, $T_{eff} = 3227/(\ln(\tau) + 6.09) + 7$ (see text for details) plotted as a function of the specific volume. The fitted equation used to produce the smooth dotted line in Figure 6 has been used to generate the smooth curve in this figure by inserting the values of τ for a particular specific volume into the relation for T_{eff}.

obtained for $n_m = 2$, 3, 5, 7, 10, and 143 fitted to the form $\tau(n_m) = \tau_\infty(1 - \exp(-\lambda n_m))$ with $\tau_\infty = 7.26$ ps and $\lambda = 0.068$. We note though that, in this case, the best-fit values of β decreased significantly with chain length, which is in agreement that the β factor is an indicator of the degree of cooperativity in the motion.[42]

The data for the $n_m = 143$ chains at 400 and 500 K were then used to obtain the constants in the Arrhenius fit to $1/\tau = C \exp(-E/RT)$, or $\ln(\tau) = -\ln(C) + E/RT$. The constants obtained, $\ln(C/\text{ps}^{-1}) = 6.09$ and $E/R = 3227$ K, could then be obtained to define an "effective" temperature, T_{eff}, for the relaxation times obtained at 343 K as a function of density for the $n_m = 30$ chains, i.e. $\tau(\rho(p\sim0),T_{eff}) = \tau(\rho,T{=}343\text{ K})$, the temperature of a system at $p \sim 0$ which has the corresponding relaxation time. This effective temperature was, therefore, defined as $T_{eff} = 3227/(\ln(\tau) + 6.09) + \Delta T$ where $\Delta T = 343 - 336 = 7$ K is the small offset required to bring the extrapolation of the $n_m = 143$ data at 400 and 500 K into agreement with the $n_m = 30$ data at 343 K. The effective temperature is plotted as a function of specific volume in Figure 7. It shows that a lowering of the density by ~10% below that of its ambient pressure value at 343 K can induce a decrease in relaxation time equivalent to as much as a ~60 K increase in temperature.

3.3.2. Self-Diffusion Coefficients. All-atom mean-square displacements, MSDs, were analyzed for each system under study over the MD production times. They are displayed in Figure 8 and show as expected that self-diffusion increases with volume. The Einstein equation can then be used to calculate the diffusion coefficients D as a function of the system density, with

$$D = \lim_{t\to\infty} \frac{1}{6t}\langle(\mathbf{r}_i(t) - \mathbf{r}_i(0))^2\rangle \qquad (7)$$

Analyses of the MSDs give diffusion coefficients of 10.6 $\times 10^{-7}$ cm^2 s^{-1} for 990 kg m^{-3}, 7.3 $\times 10^{-7}$ cm^2 s^{-1} for 1017.5 kg m^{-3}, 3.4 $\times 10^{-7}$ cm^2 s^{-1} for 1050 kg m^{-3}, 2.8 $\times 10^{-7}$ cm^2 s^{-1} for 1072.5 kg m^{-3}, and 2.6 $\times 10^{-7}$ cm^2 s^{-1} for 1110 kg m^{-3}. This order of magnitude is in good agreement with experimental data on diffusion coefficients of polymers in the bulk melt.[43] The increase in self-diffusion of the chains upon volume expansion is nonlinear with an abrupt change at lower density toward a more rapid increase in D. This sharp change in behavior is not well described by equations of the

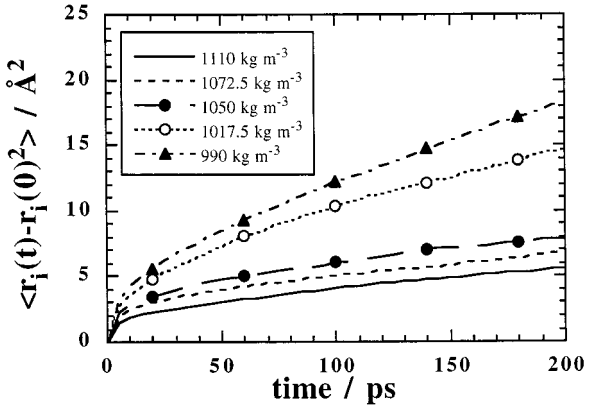

Figure 8. All-atom mean-square displacements of each system under study.

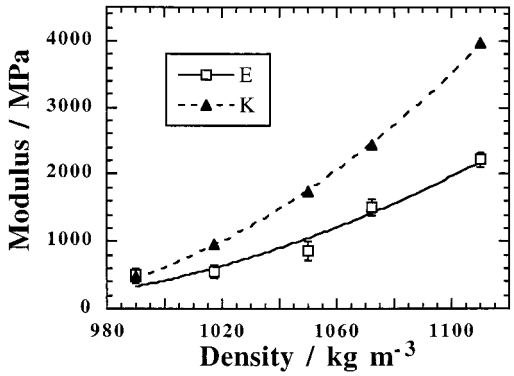

Figure 9. Young's and bulk moduli of the systems as a function of density at 343 K.

Arrhenius or WLF form. This rapid increase in diffusion is likely to be due to the combined effect of the increase in both conformational mobility and in inertial mobility, i.e. less backscattering, as the volume increases.

3.4. Mechanical Properties. To investigate the change in mechanical properties as a function of density, equilibrated configurations for each system under study were subjected to a gradually increasing uniaxial tension along the z axis by changing the z component of the applied pressure tensor at a constant rate of -2.5 MPa ps^{-1}. The response of the **h** matrix, defining the size and shape of the primary cell, and the measured pressure tensor **P** were monitored. At low strains for a system with a well-defined Young's modulus E, the measured tension $-P_{zz}$ is related to the extension γ_L by

$$-P_{zz} = E\gamma_L \qquad (8)$$

More details can be found about the computational method in ref 44. It should be noted that the Young's moduli obtained in this way depend on the rate at which the applied tension is changed. It has been shown previously that, except at very low temperatures, E decreases as the rate of applied tension is decreased,[44] as expected. It should also be noted that the rate of change of the applied tension used here leads to linear strain rates in the region of ~10^9 s^{-1}. Alternatively, this can be thought of as appertaining to frequencies in the gigahertz regime for an oscillatory experiment.

The measured tensions obtained were linear, and the corresponding Young's moduli are shown in Figure 9. They vary nonlinearly with density between ~0.5 GPa for the lowest densities and ~2.2 GPa for the bulk melt system at its ambient pressure density.

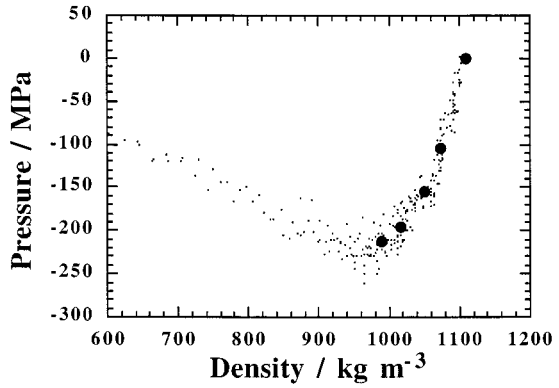

Figure 10. Pressure plotted as a function of the density as obtained from the uniaxial extension experiments; each dot represents a subaverage over a period of 2.5 ps. For comparison, the average pressures from the equilibrium simulations are also plotted as the large filled circles. The two sets of data are consistent, and the equilibrium system with the lowest density is close to the tensile limit.

A knowledge of the pressure, P, as a function of the volume, V, also allowed for the calculation of the bulk modulus, K, which is defined as

$$K = -V\left(\frac{\partial P}{\partial V}\right)_T \tag{9}$$

In this case, equilibrium data are being used so the bulk moduli obtained should be rate-independent.

The bulk modulus is also plotted as a function of density in Figure 9. It varies nonlinearly between ~0.5 GPa for the lowest density and ~4 GPa for the bulk melt system at its ambient pressure density. As K is simply the inverse of the compressibility, it must tend to zero as the tensile limit is approached.

The equilibrium values of K and the strain-rate-dependent E were then used to estimate the variation of Poisson's ratio, ν, at 343 K as a function of the density, using the following well-known relationship for isotropic systems

$$E = 3K(1 - 2\nu) \tag{10}$$

Values for the (strain-rate-dependent) Poisson's ratio obtained in this way are ~0.4 except for the lowest density which from Figure 9 is clearly closer to $^1/_3$. An alternative route to ν is via the ratio between the contractile and extensile strains (results not shown), and although this is subject to large errors at small extensions, the main point that emerges from either route is that Poisson's ratio falls sharply as we get close to the tensile limit. If the system were actually *at* the tensile limit, any extension would lead to the system pressure becoming *less* negative, thus removing the tendency for contraction in the transverse directions. A direct consequence of which is that Poisson's ratio at the tensile limit must be zero or negative. Some confirmation that the lowest density system is close to this limit can be discerned from the density vs pressure data for the systems subjected to uniaxial tension. Although not strictly comparable, we plot in Figure 10 all the nonequilibrium data along with that obtained at equilibrium. The data are, however, quite consistent with each other and demonstrate clearly the passage of the pressure through a minimum value close to that of the lowest density equilibrium system studied.

It should be noted that Young's moduli of the order of 1 GPa and Poisson's ratio of ~0.4 would indicate that our material is responding in the "leathery" regime of behavior close to the glassy regime, rather than in the rubbery state. This is due to our high deformation rates, and one could suggest conducting the MD at a significantly higher temperature in order to use realistic deformation rates. If we increase the temperature, we will indeed reduce the viscosity. However, as the limiting factor in the nonequilibrium MD experiment is the level of stress generated, lowering the viscosity necessarily implies higher strain rates. This is a technical limitation of nonequilibrium MD simulations of relatively small samples.

Experimentally, it is known that Poisson's ratio generally increases with temperature at constant pressure, i.e., as the volume increases. It is reasonable to assume that decreasing, *but positive*, pressures, i.e., increasing volume, has the same effect at constant temperature. This combined with the above leads to the implication that Poisson's ratio must pass through a maximum somewhere between zero and the tensile limit. This latter point is important as it has been previously noted that a small decrease in the interphase Poisson ratio influences strongly the position of the "micromechanical transition" in the theoretical DMS of compatibilized thermoplastic blends.[5] Our results seem to confirm that a volume increase at the interphase of the blend can indeed be linked with such a transition.

4. Conclusion

This work was initiated by the observation of a new peak, called a "micromechanical transition", at about 343 K in the mechanical spectrum of immiscible PMMA/PPO polymer blends compatibilized with a graft P(S-*g*-EO) polymer.[6] Moreover, the occurrence of this "micromechanical transition" was found to be related to the expansion of the interphase.[9] As a first step, a previously well-tested MD model for PEO[11−13] was used to study the structure and mobility of this polymer at the molecular level in response to a volume expansion such as might occur at the interphase of the blends. Bulk melt PEO was simulated at densities in the wide range from ~90% to 100% of its ambient pressure density at 343 K in order to follow the evolution of its physical properties as a function of density and to establish quantitative trends. It is worth emphasising that such experiments would be difficult to realize in the laboratory whereas they are relatively straightforward to perform using atomistic MD simulation.

As volume expands, thermodynamic properties are dominated by the loss in cohesive van der Waals energy. The simulated pressure decreases nonlinearly with increasing specific volume and tends toward a minimum value in the region of −220 MPa at a density of 990 kg m^{-3}. Structural properties show variations with a marked tendency for increased stability of intramolecular torsional states for OCCO and CCOC dihedral angles as density decreases. Intermolecular distances are scaled in an affine manner at large separations, but intermolecular nearest-neighbor distances display more of an intramolecular-type behavior, preferring to remain at the same distances in the energy wells. Dynamic properties such as conformational mobility and diffusion are very much affected by lower densities. Indeed, the self-diffusion coefficient is multiplied 4-fold for a density of 990 kg m^{-3}. Translating the change of COCC relax-

ation times with volume into an equivalent change in temperature gives up to a 60 K temperature shift for the lowest density. The Young's and bulk moduli decrease nonlinearly upon volume expansion. In addition, the behavior of Poisson's ratio is especially interesting with respect to the "micromechanical transition", which was found to be directly linked to small variations in the interphase Poisson's ratio.[5] It is not possible at this stage to conclude whether negative pressures produced in the interphase between the vitreous PMMA and PPO regions are responsible for the phenomena observed in DMS experiments of these systems.[5] However, this study shows clearly that such effects are consistent with a volume expansion of the interphase.

Further work could involve the creation of a full graft P(S-*g*-EO) interphase by combining a PS and a PEO model and comparing results at various densities with those presented here. Also of interest are molecular interactions at the PPO/PS and PEO/PMMA interfaces. This requires large simulations with very complex potentials and has to be done on a step-by-step basis. It can, however, provide complementary information to experiment on interfaces in multiphase materials.

Acknowledgment. The IDRIS (Orsay, France) and the CNUSC (Montpellier, France) computer centers are acknowledged for the provision of computer time on the Cray T3E and on the IBM SP2. We also acknowledge helpful discussions during the course of this work with Dr. Mataz Alcoutlabi.

References and Notes

(1) Yu, A. J. *Multicomponent Polymer Systems*; N. A. J. Platzer: Washington, DC, 1971.
(2) Gaylord, N. G. *Copolymers, Polyblends and Composites*; N. A. J. Platzer: Washington, DC, 1975.
(3) Gedde, U. W. *Polymer Physics*; Chapman & Hall: London, 1995.
(4) Chen, C. C.; White, J. L. *Polym. Eng. Sci.* **1993**, *33*, 923.
(5) Eklind, H.; Maurer, F. J. H. *Polymer* **1996**, *37*, 2641.
(6) Eklind, H.; Schantz, S.; Maurer, F. H. J.; Jannasch, P.; Wesslen, B. *Macromolecules* **1996**, *29*, 984.
(7) Eklind, H.; Maurer, F. H. J. *J. Polym. Sci., Part B: Polym. Phys.* **1996**, *34*, 1569.
(8) Eklind, H.; Maurer, F. H. J.; Steeman, P. A. M. *Polymer* **1997**, *38*, 1047.
(9) Colombini, D.; Merle, G.; Martinez-Vega, J. J.; Girard-Reydet, E.; Pascault, J. P.; Gerard, J. F. *Polymer* **1999**, *40*, 935.
(10) Allen, M. P.; Tildesley, D. J. *Computer Simulation of Liquids*; Clarendon Press: Oxford, 1987.
(11) Neyertz, S.; Brown, D.; Thomas, J. O. *J. Chem. Phys.* **1994**, *101*, 10064.
(12) Brown, D.; Neyertz, S. *Mol. Phys.* **1995**, *84*, 577.
(13) Neyertz, S.; Brown, D. *J. Chem. Phys.* **1995**, *102*, 9725.
(14) Jackson, C. L.; McKenna, G. B. *J. Non-Cryst. Solids* **1991**, *131*−*133*, 221.
(15) Zhang, J.; Liu, G.; Jonas, J. *J. Phys. Chem.* **1992**, *96*, 3478.
(16) Angell, C. A.; Qing, Z. *Phys. Rev. B* **1989**, *39*, 8784.
(17) Kieffer, J.; Angell, C. A. *J. Non-Cryst. Solids* **1988**, *106*, 336.
(18) Mausbach, P.; Schnitker, J.; Geiger, A. *Z. Angew. Math. Mech.* **1994**, *74*, T608.
(19) Weber, T. A.; Helfand, E. *J. Chem. Phys.* **1980**, *72*, 4014.
(20) Neyertz, S.; Brown, D.; Clarke, J. H. R. *J. Chem. Phys.* **1996**, *105*, 2076.
(21) Brown, D.; Clarke, J. H. R.; Okuda, M.; Yamazaki, T. *J. Chem. Phys.* **1994**, *100*, 1684.
(22) Brown, D.; Clarke, J. H. R.; Okuda, M.; Yamazaki, T. *J. Chem. Phys.* **1994**, *100*, 6011.
(23) Neyertz, S.; Brown, D. *J. Chem. Phys.* **1996**, *104*, 10063.
(24) Roe, R. J. *J. Phys. Chem.* **1968**, *72*, 2013.
(25) Van Krevelen, D. W. *Properties of polymers: their correlation with chemical structure; their numerical estimation and prediction from additive group contributions*, 3rd completely revised ed.; Elsevier: Amsterdam, 1990.
(26) Brown, D. *the gmq manual*, 1999. Available from http://www.univ-savoie.fr/labos/lmpc/gmq.html.
(27) Brown, D.; Minoux, H.; Maigret, B. *Comput. Phys. Commun.* **1997**, *103*, 170.
(28) Brown, D.; Clarke, J. H. R. *Comput. Phys. Commun.* **1991**, *62*, 360.
(29) Fincham, D. *Inf. Q. Comput. Simul. Condens. Phases* **1993**, *38*, 17.
(30) Berendsen, H. J. C.; Postma, J. P. M.; van Gunsteren, W. F.; DiNola, A.; Haak, J. R. *J. Chem. Phys.* **1984**, *81*, 3684.
(31) Berthollet, M. *Ann. Chim. (Phys.)* **1850**, *30*, 232.
(32) *Polymer Handbook*, 3rd ed.; Wiley-Interscience: New York, 1989.
(33) Schmidt, M.; Maurer, F. H. J. *J. Polym. Sci., Part B: Polym. Phys.* **1998**, *86*, 1061.
(34) Simha, R.; Somcynsky, T. *Macromolecules* **1969**, *2*, 342.
(35) Tait, P. G. *Phys. Chem.* **1988**, *2*, 1.
(36) Müller-Plathe, F. *Acta Polym.* **1994**, *45*, 259.
(37) Müller-Plathe, F.; van Gunsteren, W. F. *Macromolecules* **1994**, *27*, 6040.
(38) Brown, D.; Clarke, J. H. R. *J. Chem. Phys.* **1990**, *92*, 3062.
(39) Gejji, S. P.; Tegenfeldt, J.; Lindgren, J. *Chem. Phys. Lett.* **1994**, *226*, 427.
(40) Williams, G.; Watts, D. C. *Trans. Faraday Soc.* **1970**, *66*, 80.
(41) Neyertz, S.; Brown, D.; Thomas, J. O. *Comput. Polym. Sci.* **1995**, *5*, 107.
(42) Ngai, N. L.; Randall, R. W.; Rajagopal, A. K.; Teitler, S. *Ann. N. Y. Acad. Sci.* **1986**, *484*, 150.
(43) Sperling, L. H. *Introduction to Physical Polymer Science*; John Wiley and Sons: New York, 1986.
(44) Brown, D.; Clarke, J. H. R. *Macromolecules* **1991**, *24*, 2075.

MA990927N